IEEE Photonics Journal
An IEEE Photonics Society Publication

Open Access

Optically Integrated InP–Si_3N_4 Hybrid Laser

Volume 8, Number 6, December 2016

Youwen Fan
Jörn P. Epping
Ruud M. Oldenbeuving
Chris G. H. Roeloffzen
Marcel Hoekman
Ronald Dekker
René G. Heideman
Peter J. M. van der Slot
Klaus-J. Boller

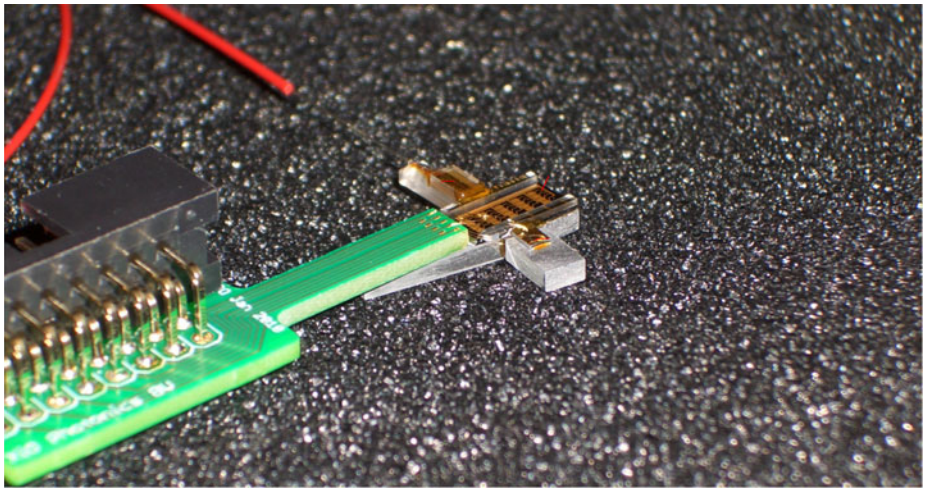

DOI: 10.1109/JPHOT.2016.2633402
1943-0655 © 2016 IEEE

Optically Integrated InP–Si_3N_4 Hybrid Laser

Youwen Fan,[1] Jörn P. Epping,[2,3] Ruud M. Oldenbeuving,[2,3] Chris G. H. Roeloffzen,[2,3] Marcel Hoekman,[3] Ronald Dekker,[4] René G. Heideman,[3] Peter J. M. van der Slot,[1] and Klaus-J. Boller[1]

[1]University of Twente, MESA+ Institute for Nanotechnology, Laser Physics and Nonlinear Optics Group, Enschede 7500 AE, The Netherlands
[2]SatraX B.V., Enschede 7500 AL, The Netherlands
[3]LioniX B.V., Enschede 7500 AL, The Netherlands
[4]XiO Photonics B.V., Enschede 7500 BG, The Netherlands

DOI:10.1109/JPHOT.2016.2633402

Manuscript received October 24, 2016; revised November 22, 2016; accepted November 23, 2016. Date of publication December 1, 2016; date of current version December 14, 2016. This work is funded within the framework of the Promis2Day project, supported by the IOP Photonic Devices program of Rijksdienst voor Ondernemend Nederland: a part of the Netherlands Ministry of Economic Affairs and the Netherlands Ministry of Education, Culture and Science. Corresponding author: Y. Fan (e-mail: y.fan@utwente.nl).

Abstract: We describe the first demonstration and characterization of an optically integrated InP–Si_3N_4 hybrid laser. The laser is formed by integration of an InP-based reflective semiconductor optical amplifier with a Si_3N_4 based feedback waveguide circuit. The circuit comprises a frequency selective and tunable Vernier mirror composed of two microring resonators with slightly different radii. A wide tuning range of more than 43 nm is achieved via the thermo-optic effect. The typical side mode suppression ratio is 35 dB. The narrowest linewidth achieved is about 90 kHz, and the relative intensity noise is less than −135 dBc/Hz.

Index Terms: Tunable lasers, semiconductor lasers, waveguide devices.

1. Introduction

There has been an ever-increasing demand for higher bandwidth in fiber-optic communications. Such demand has driven the need for integrated semiconductor laser sources with narrow linewidths that can be applied in dense wavelength division multiplexing (DWDM) using advanced modulation formats, such as quadrature amplitude modulation (QAM) [1]. Besides fiber-optic telecommunications, applications that benefit from such lasers are optical beamforming networks [2], light detection and ranging (LIDAR) [3], spectroscopy [4], optical sensing [5] or space-based laser cooling [6], and atomic clocks [7] in global positioning systems (GPS). Especially when looking for narrow spectral bandwidth, monolithic semiconductor lasers, where all the components of the laser are made of the same materials, approach their limits. This is the reason why so-called hybrid lasers are currently gaining considerable interest. In such lasers, a semiconductor amplifier made of active material providing optical gain is optically coupled to an integrated optical waveguide circuit fabricated from a different passive material (without optical gain). Specifically, replacing any passive but otherwise relatively lossy section of a semiconductor waveguide resonator by low-loss passive waveguides enables reducing the total cavity loss and increasing the cavity length, which is known to decrease the Schawlow-Townes linewidth of the laser [8].

The hybrid laser schemes investigated so far can be divided into three types: a) evanescently coupled III/V on Si lasers [9]; b) lasers which utilize a vertical taper to realize an adiabatic conversion of the optical mode from a III-V gain waveguide into passive waveguides [10]–[12]; and c) reflective semiconductor optical amplifiers (RSOAs) butt-coupled to external waveguide circuits, realized with various passive waveguide platforms such as Si [13], [14], SiON [15], polymer [16], and Si_3N_4 [17]. While evanescently and adiabatically coupled lasers might be integrated via bonding techniques, they require sophisticated fabrication technology which essentially introduces III-V material in CMOS processing lines, which is generally not supported in current foundries. Moreover, the passive material used so far has exclusively been limited to Si, and thus to certain infrared ranges including the telecom range while, but excluding applications in the visible. The third type, however, is quite different in that it relieves the difficulties in fabrication and broadens the choice of materials. The RSOA and external waveguide circuitry can be fabricated separately, for achieving high performance with independently optimizing each component.

Recently we have reported the first demonstration of an RSOA butt-coupled semiconductor-Si_3N_4 hybrid laser where frequency selection is achieved using a Vernier mirror based on two microring resonators (MRRs) [17], [18]. Using an InP based RSOA, held next to the Si_3N_4 chip with alignment stages, a wide tuning range covering the entire telecom C-band was achieved. The emerging Si_3N_4 waveguide platform is of special importance because it can offer some fundamental and technological advantages over other passive waveguide platforms: a) compared to silica that has only a low index contrast (Δ n $\approx 10^{-2}$ [19]), the index contrast is very high, Δ n $\approx$ 0.5, rendering a small footprint achievable even with long optical lengths; b) Si_3N_4 waveguides provide a very large transparency range, from 400 nm to 2400 nm [20], which means that a large varieties of semiconductor materials other than InP might be used, to form hybrid lasers working at other wavelengths including the visible range; c) very low linear propagation loss in the order of 0.1 dB/cm [21] when using a double-stripe cross-section and record-low loss of less than 0.001 dB/cm with a single-stripe cross-section [22]; d) its low nonlinearity, which prevents two-photon absorption [23]; e) its maturity in terms of design, tunability [24] and programmability [25], which enables access to complex functionalities on the same photonic chip.

The aforementioned advantages of a hybrid InP-Si_3N_4 laser call for a feasible approach to integrate such lasers, which is the key for applications. Examples are flip-chip bonding [26]–[28] and a recently reported 3-D integration utilizing a total internal reflection (TIR) turning mirror within the RSOA [29]. However, those approaches require a highly specific design of the RSOA, ruling out the possibility of utilizing off-the-shelf, standard gain chips that are easily available at most desired wavelengths and powers.

In this paper, we demonstrate an optically integrated InP-Si_3N_4 laser for the first time. A first challenge in this, when using standard, non-customized RSOA chips and basic, non-tapered waveguides, is that even with perfect alignment the optical mode mismatch can be large and cause coupling loss at the 90% level [17]. Tapered waveguides would increase the optical coupling but different tapers are required for different types of RSOAs which deviate significantly in their mode field diameters (MFD). Second, the typical limit in alignment accuracy is in the order of 0.1 μm which introduces unforeseeable loss particularly at small and well-matched mode field diameters. These effects greatly influence the the achievable output power via an unknown increase in laser threshold, in addition to threshold variations due to the spectrally varying transmission of the output mirror which is a major aspect of laser cavity designs [14]. Ruling out these shortcomings and uncertainties and improving accuracy in positioning and fixation is certainly possible to an appreciable extent but it would lead to smaller tolerances and thus higher risk and costs in optical integration.

In this work, the goal is to demonstrate a viable way of integrating a hybrid laser that offers useful output power at the mW-level and still provides a large tolerance to the named losses, although this would sacrifice wall plug efficiency and increases the spectral linewidth of the laser [8]. To secure a strong loss margin, we use an RSOA with a rather large length to provide high gain. Numerical modeling of the output power versus coupling loss is carried out to quantify our assumption of the loss margin, while comparison with experimental output data can be used to determine the amount of losses present. After integration of the hybrid laser, its spectral linewidth and other important

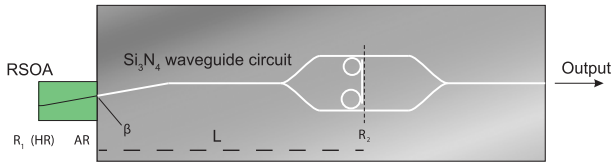

Fig. 1. Schematic drawing of the hybrid laser (not to scale). R_1 is the reflectivity of the high reflection (HR) coated amplifier back facet, R_2 is the overall reflectivity of the Vernier mirror, L is the total length of the feedback circuit, and β is the power coupling efficiency between the anti-reflection (AR) coated diode waveguide and the Si_3N_4 waveguide.

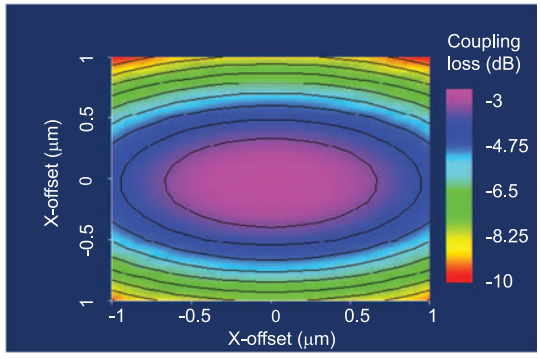

Fig. 2. Calculated coupling loss between the InP RSOA chip and the Si_3N_4 chip as a function of transverse misalignment. It can be seen that the optimum coupling loss is about 2.6 dB. The 1-dB misalignment tolerance reaches 1.6 μm in the horizontal direction and 1.3 μm in the vertical direction.

properties, such as the side mode suppression ratio (SMSR) and relative intensity noise (RIN), are presented.

2. Device Description and Operation Principle

The basic waveguide layout of the hybrid laser under investigation is shown in Fig. 1. The laser comprises an InP based RSOA and a Si_3N_4 waveguide circuit. The RSOA (obtained from the Fraunhofer Heinrich-Hertz-Institute, Berlin) possesses a relatively long length of 2 mm, in order to provide a high single-pass gain for compensating potential high losses in the hybrid laser cavity. The RSOA has a HR coated back-facet with a reflectivity of $R_1 = 90\%$ and an AR coating of the front-facet optimized for a refractive index of 1.5, close to the effective index of the external Si_3N_4 waveguide which was used in this work (1.535). The diode waveguide is angled with regard to the front facet by 9° to further reduce perturbing back reflection. This was successfully achieved, because the output spectra as presented later, appear free of a 0.16-nm modulation that would correspond to the optical roundtrip length of the diode; the MFD is specified to be 4.2 μm in the horizontal direction and 1.95 μm in the vertical direction. These values for the MFD are large when compared with other commercially available RSOA chips and also compared with the MFD of the Si_3N_4 waveguide used here (1.62 μm in the horizontal direction and 1.72 μm in the vertical direction). Although this mismatch will lead to increased roundtrip losses of the hybrid laser, the purpose here is to improve the tolerance *vs* misalignment. The calculated coupling loss between the two chips as a function of transverse misalignment is shown in Fig. 2. It can be seen that the coupling loss increases by 1 dB with a misalignment of 1.6 μm in the horizontal direction or 1.3 μm in the vertical direction. Given that state-of-the-art precision stages that we use here provide 100 nm resolution, a sufficiently large misalignment tolerance should be present. The RSOA chip is butt-coupled to the Si_3N_4 waveguide circuit, which carries a circuitry composed of two cascaded (Vernier) MRRs that work as highly frequency selective feedback elements for imposing

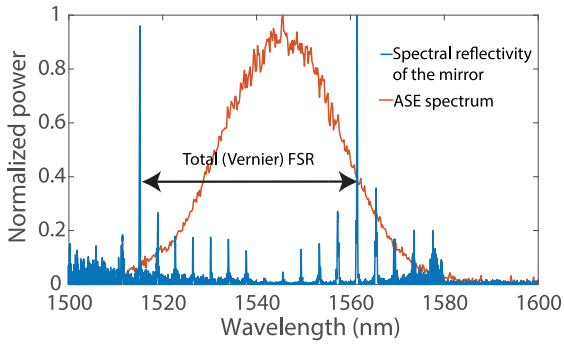

Fig. 3. Amplified spontaneous emission (ASE) spectrum (red curve) of the RSOA at 80 mA driving current is displayed together with the spectral reflectivity (blue curve) of the Vernier mirror when using a superluminescent diode (SLD) as the light source. Both spectra are normalized to their corresponding maxima.

single-frequency operation at a narrow spectral bandwidth. The two slightly different radii of the MRRS and their power coupling coefficients are selected such that a) the total free spectral range (FSR) of the Vernier mirror exceeds the gain bandwidth of the RSOA, and b) that the spectral side peaks of the Vernier mirror reflectivitiy are suppressed to avoid lasing at undesired side modes [17].

For checking the fulfillment of these conditions we measured the amplified spontaneous emission (ASE) spectrum of the RSOA and the reflection spectrum of various Vernier mirrors. An example of an ASE spectrum is shown in Fig. 2, recorded at a driving current of 80 mA. The reflectivity of the Vernier mirror selected for laser feedback (MRR radii of 49.5 and 54.0 μm, power coupling coefficients set to 0.3, total circuit length L = 3.5 mm) was measured with a broadband (3 dB spectral width of 50 nm) superluminescent diode (SLD) and is plotted in Fig. 3 as well. It can be seen that the RSOA provides optical gain over more than 35 nm bandwidth, covering the telecom C-band and that the Vernier mirror exceeds this bandwidth with a total free spectral range (FSR) of 46.4 nm and high side peak suppression.

3. Modeling of the Output Power versus Coupling Efficiency β

In order to retrieve important parameters that are needed for modeling the output power of the hybrid laser under various coupling efficiencies, β, first, the RSOA output power (as cleaved, before the deposition of HR and AR coatings) *vs* driving current (LI curve) was recorded in solitary operation, i.e., before integration with the Si_3N_4 circuit. From the LI curve that showed a threshold current of 50 mA and slope efficiency of about 13.5%, we calculated a gain-factor g_0 of 2550 cm^{-1} and an internal loss coefficient of 12.55 cm^{-1}, using a rate equation (RE) model [31] when the tilting induced reflectivity (16.5%) is taken into account [30]. g_0 is the current-independent gain-factor that scales in the gain coefficient g, as follows: $g = g_0 \ln N/N_{tr}$, where N is the carrier density which depends on driving current, and Ntr is the transparency carrier density.

To verify that the chosen high-gain RSOA provides a high tolerance with regard also to higher losses between the InP and the S_3N_4 interface, and for a later comparison with the experimental output power in order to evaluate the value for β that was actually achieved, we calculated the LI characteristics of the hybrid laser for different values of the coupling efficiency. Using the RE model, a wide range from weak coupling ($\beta = 0.1$), medium ($\beta = 0.5$) to perfect coupling ($\beta = 1$), was considered in the calculations whereas the RSOA back reflection was taken as equal to the specified value $R_1 = 90\%$ and the effective Vernier feedback as $R_2 = 90\%$. The calculated power *vs* driving current at various values of β is shown in Fig. 4. It can be seen that the slope efficiency only varies by a factor of two although the coupling loss varies by a factor of ten, from $\beta = 0.1$ to 1. This differs significantly from the calculated result in [26], where a much shorter (600 μm) RSOA was used. An explanation can be that in their case the coupling loss is dominating

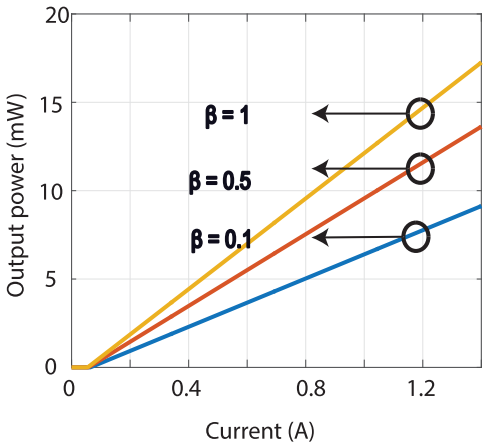

Fig. 4. Numerically calculated LI curves at different optical coupling efficiencies β.

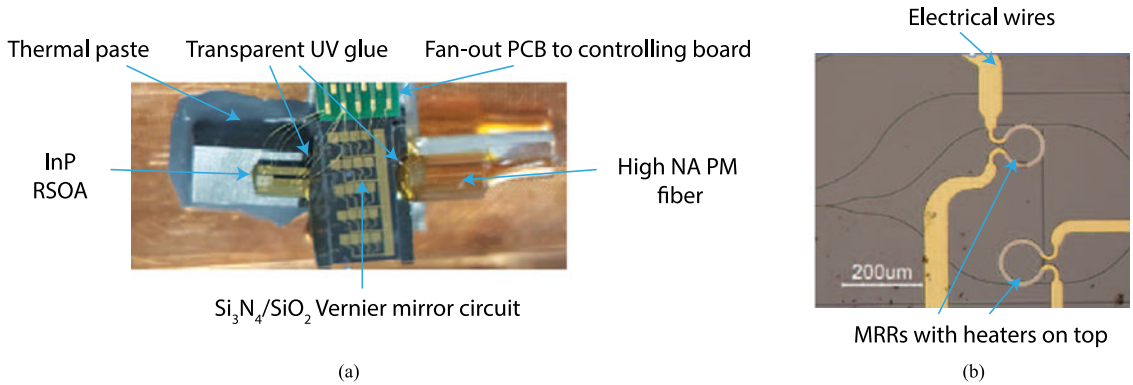

Fig. 5. (a) Integrated hybrid laser. (b) Microscope image of the Vernier mirror.

the roundtrip loss, such that the change of slope efficiency is comparable to the change of β. In our case it can be seen that the hybrid laser should, although at high currents, provide an output in the 10 mW-range, even if the coupling becomes very small ($\beta = 0.1$). Recalling that $\beta = 0.1$ means 99% power loss per roundtrip shows that a high-gain RSOA indeed introduces a huge tolerance in terms of β. The latter proved important for successful laser operation with the integration procedure described as follows, which has not been evaluated so far. We note that the previously investigated version of the laser was still based on manually aligning the two chips with precision stages during characterization of the laser output.

4. Integration Processes

A close-up and microscope photograph of the integrated laser is shown in Fig. 5. The RSOA chip and the chip with the feedback circuit were fixed on separate submounts and held by two precision translation stages. The electric contact pads of the MRRs were wire-bonded to a fan-out printed circuit board (PCB) which is connected to a dedicated controlling board. Low currents were injected in the InP RSOA via probe needles to generate an ASE output for next alignment steps. The output waveguide facet of the feedback chip was first aligned and assembled with a high numerical aperture (NA) polarization maintaining (PM) fiber. The specified 1/*e* mode field diameter (MFD) of the fiber is 6 μm in both directions, which is close to the MFD of the output waveguide (about 5 μm in both directions). A small amount of optically transparent UV curable glue was applied to

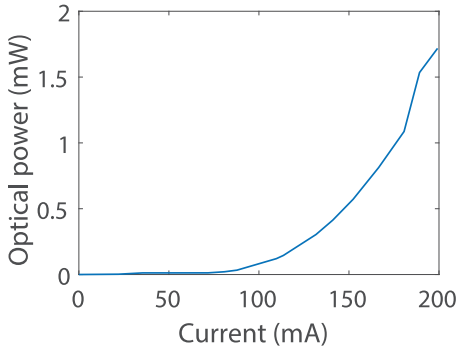

Fig. 6. Measured output power vs driving current of the hybrid laser.

the InP-Si_3N_4 interface. As a next step the InP RSOA and Si_3N_4 circuit were aligned relative to each other using translational stages while the fiber-coupled output ASE power of the hybrid laser is monitored and maximized as a signature for best optical coupling, i.e., a maximized value for β. UV light was used to cure the adhesive after the optimum alignment was obtained, thereby fixing the two components at best optical alignment. As the second step after curing of the UV glue, the InP-Si_3N_4 hybrid laser assembly was taken off the alignment stages and fixed on top of a copper heat sink using thermal paste, which allows driving currents of up to 200 mA before thermal effects set in.

5. Characteristics of the Integrated Hybrid Laser and Discussion

We measured the output characteristics of the integrated hybrid laser to evaluate whether laser oscillation is achie-ved after after integration. In brief, as will be discussed below, we achieved single-mode laser oscillation with mW-level output power with wide tunability, narrow linewidths, good side-mode suppression ratio and low intensity noise.

5.1 Output Power vs Driving Current

In the experiments performed at room temperature, the laser showed a threshold current of approximately 70 mA and an output power of 1.7 mW, obtained at the maximum applicable driving current of 200 mA, as is shown in Fig. 6. These results match well with the calculated LI curve at $\beta = 0.5$ in Fig. 4. Calculations revealed that this value is close to what is obtained from calculation of the RSOA-Si_3N_4 field overlap integral alone ($\beta = 0.6$). This indicates that the alignment and integration precision have not been the major limiting factor. The wall plug efficiency achieved here (0.85%) is comparable with our previous work [17], where an efficiency of 0.96% was achieved. As a consequence a further increase in the mode matching appears promising for increasing the output power in a next step.

5.2 Wavelength Tuning

The laser output wavelength was tuned via phase shifters on top of the MRRs. Here, we have used thermal tuning based on two resistive heaters (one for each MRR) using a maximum power of about 250 mW. It should be noted that in this waveguide platform piezo-tuning has been demonstrated as well [32] which can strongly reduce the required power. Fig. 7 shows both coarse and fine tuning. It can be seen that the hybrid laser offers a broad tuning range of more than 43 nm. To more detail, Fig. 7(a) shows the case when only one of the two MRRs was tuned. This gives rise to discrete changes of the laser wavelength at a stepsize of the FSR of the other MRR (in this case, $\Delta\lambda = 4$ nm). We note that this measurement was solely intended to determine the

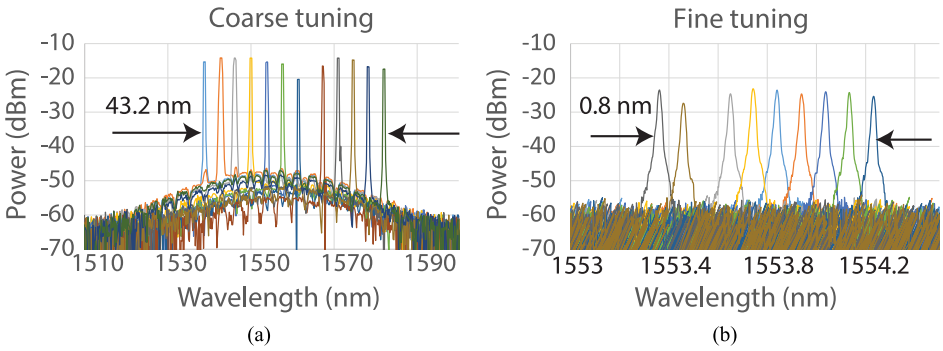

Fig. 7. (a) Superimposed spectra when coarsely tuning over a 43 nm wide range as observed when thermally tuning only one of the two MRRs. (b) Superimposed spectra when fine-tuning over a range of 0.8 nm via tuning both MRRs simultaneously, achieving a stepwise sweeping of the wavelength at the FSR of the whole laser cavity.

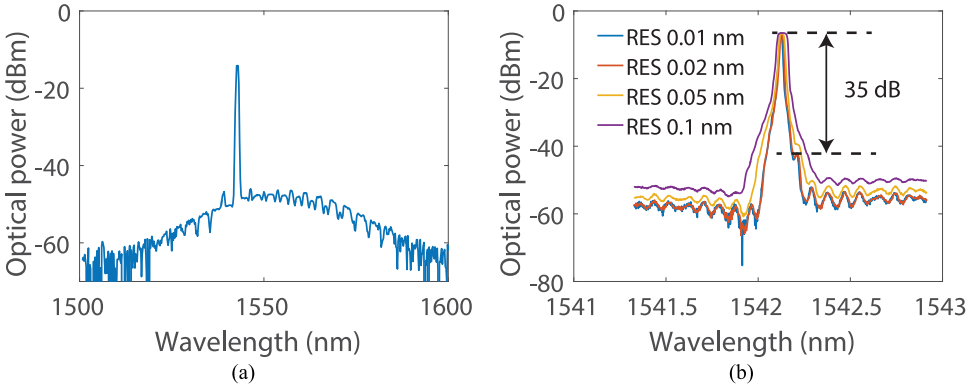

Fig. 8. (a) Single mode output spectrum measured at a resolution of 1 nm, at a driving current of 90 mA. (b) Same spectrum recorded with higher resolution (RES) around the laser wavelength. It is noted that the SMSR (35 dB) is well-resolved at resolutions better than 0.02 nm.

maximum tuning range (yielding a value of 43.2 nm). A detailed analysis of the displayed output power vs wavelength remained difficult due to the manual tuning procedure and limitations to the heater current (damage). For tuning, the heating current was manually increased until a mode hop occurred. Then some adjustment of the heating current was used to roughly maximize the output power at that wavelength, thereafter proceeding to the next mode hop. The wavelength in the middle of the tuning range (near 1560 nm), where the output power was 6 dB less, was actually achieved with the maximum allowable heating current, where a fine adjustment was not possible anymore. Fig. 7(b) shows the case when both MRRs were tuned simultaneously, which allows for a much finer tuning stepsize of $\Delta\lambda = 0.09$ nm. The latter value corresponds to the FSR of the entire laser cavity, i.e., in this tuning mode, the laser performs axial mode hops. A finer tuning might possibly be achieved either with a finely controlled change of the diode driving current or, alternatively, with implementing an additional phase tuning section in the Si_3N_4 waveguide circuit.

5.3 Side Mode Suppression Ratio

In order to characterize the hybrid laser's side-mode suppression ratio (SMSR), we investigated the output spectrum of the laser over a wide range around the central emission wavelength. To ensure a well-resolved SMSR we performed the measurement *vs* increasing resolution of the used optical spectrum analyzer (OSA) (ANDO, AQ6317). Fig. 8(a) shows, as an overview, the measured

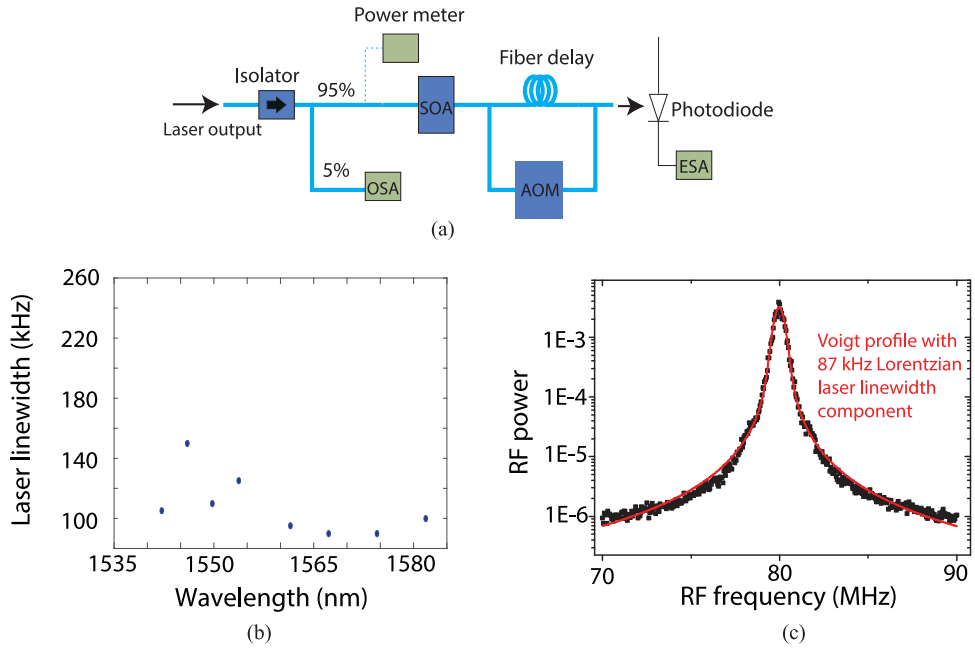

Fig. 9. (a) Schematic of the delayed self-heterodyne (DSH) detection setup for linewidth measurement. (b) Laser linewidth measured at various wavelength within the tuning range. (c) Recorded beat signal (black) at a driving current of 196 mA and a laser output wavelength of 1578.12 nm. The red fit curve represents a Voigt profile of which the Lorentzian component corresponds to an instantaneous (intrinsic) laser linewidth of 87 kHz.

typical laser spectrum over a range of 100 nm centered at 1550 nm with a coarse resolution of 1 nm. A single peak of laser output is observed on top of some background that originates from ASE emission and is filtered by the transmission spectrum of the Vernier mirror. Fig. 8(b) displays a zoom-in view of the same spectrum with four values of stepwise increased resolution, from 0.1 nm to 0.01 nm. It can be seen that the recorded spectra start to become identical towards increased resolution, i.e., at 0.02 nm and 0.01 nm. The SMSR amounts to 35 dB with regard to the nearest side mode and to values between 45 and 55 dB with regard to the other side modes, clearly indicating single-mode oscillation.

5.4 Spectral Linewidth

The spectral linewidth of the integrated hybrid laser output was too narrow to be resolved with the resolution of the OSA. For providing a higher resolution, we applied delayed self-heterodyne (DSH) detection [33], as shown in Fig. 9(a). A 6 km long fiber delay line forms the first arm of a Mach-Zehnder interferometer while an acoustic-optical modulator is placed in the other arm to induce a frequency shift of 80 MHz. The optical (short-term, instantaneous) linewidth of the laser can be retrieved by analyzing the RF beat power spectrum which is recorded by an electrical spectrum analyzer (ESA). In order to rule out spectral broadening of the laser output via pickup noise in the diode laser driving current, the laser was operated with an ultra-low noise battery current source.

We measured the linewidth at different driving currents and different laser wavelengths, since the linewidth is power dependent and wavelength dependent, due to a wavelength dependence of the linewidth enhancement factor and the laser threshold [34]. This is shown in Fig. 9(b), which that displays the variation in linewidth as recorded in search of the lowest possible value Fig. 9(c) shows the beat spectrum recorded at a driving current of 196 mA and a laser output wavelength of 1578.12 nm, for that lowest value which occurred. To extract the instantaneous linewidth [35], we fitted a Voigt profile to the spectrum. The fit yields a linewidth of 87 kHz.

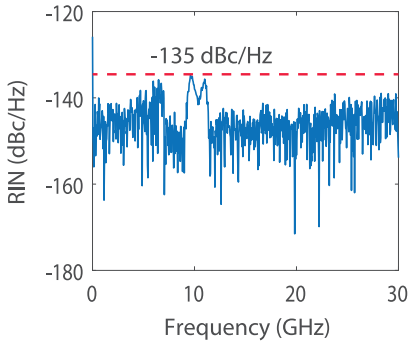

Fig. 10. Measured relative intensity noise (RIN) spectrum.

The total quality factor of the Vernier filter as measured with a second sample of the feedback chip was 7750. Inserting into Henry's formula [8] (modified for external cavity diode lasers [36]) the experimental parameters and loss parameters derived with the mean-field model [31] we find a linewidth between 8 and 28 kHz, depending on the alpha-factor (4 to 8 [37], respectively). This is smaller than the measured linewidths but may be due to other uncertainties, specifically the unknown spontaneous emission factor in [8], the wavelength-depending output coupling or the validity of the mean-field approximation in [8].

The measured linewidth value is about 4-times higher than our previously reported value of 24 kHz for a non-integrated laser [18] with a tapered Si_3N_4 waveguide for an optimized mode matching. The larger linewidth in the present experiment can be qualitatively understood to a first part from a higher coupling loss. Second, due to the increased length of the RSOA used here, one expects increased roundtrip losses, as well as a stronger influence of the linewidth enhancement factor [8]. Nevertheless, the measured linewidth compares favorably with the approximate 1-MHz linewidth of typical monolithic DBR and DFB laser sources [38], [39].

5.5 Relative Intensity Noise

To characterize the stability of the output intensity, we measured the relative intensity noise (RIN) spectrum of the hybrid laser. A fast photodiode with 20 GHz bandwidth was used for light detection and the RF signal was fed into an ESA. Fig. 10 presents a typical example of the measured RIN spectrum, recorded at 170 mA driving current, and a video bandwidth (VBW) of 100 kHz and a resolution bandwidth (RBW) of 10 kHz. It can be seen that the RIN is below a value of −135 dBc/Hz over the DC-to-20 GHz range accessible to us. Two noise peaks at 9.6 GHz and 11 GHz, via comparison with the measured optical spectrum, can be ascribed to a beating of adjacent modes, possibly in connection with a non-uniform mode spacing induced by group delay dispersion near the MRR resonances [40].

6. Conclusion

In this paper, an integrated InP-Si_3N_4 hybrid laser is demonstrated and characterized for the first time. The results from characterization of the laser confirm both the flexibility and viability of our laser integration approach, which is of high relevance for the potential application of such Si_3N_4-based hybrid lasers. In terms of improvement, there are two possible routes, which is best explained by looking at Fig. 4. By gradually improving alignment precision and implementing tapers for improved mode matching, one might attain the same amount of output power in combination with a further decreased linewidth at the 20-kHz-level [17], [18], if using a shorter RSOA, specified with a lower maximum current. A shorter RSOA enables a lower electric power consumption with less heat generation, which is an important requirement for many applications. Alternatively it might be

useful to maintain using a long RSOA with high gain if an improved cooling can be provided. Fig. 4 suggests that a factor of ten increase in the output power might be achieved at high driving currents. Considering that the linewidth reduces inversely proportionally with increasing output power [41], [42], a linewidth reduction by a factor of ten might be possible, yielding linewidths at the ten-kHz level.

Acknowledgment

The authors would like to thank the Fraunhofer Heinrich Hertz Institute for generously providing the prototype RSOA that was used in this work.

References

[1] S. Zhang, P. Y. Kam, C. Yu, and J. Chen, "Laser linewidth tolerance of decision-aided maximum likelihood phase estimation in coherent optical M-ary PSK and QAM systems," *IEEE Photon. Technol. Lett.*, vol. 21, no. 15, pp. 1075–1077, Aug. 2009.
[2] L. Zhuang *et al.*, "Novel ring resonator-based integrated photonic beamformer for broadband phased array receive antennas—Part II: Experimental prototype," *J. Lightw. Technol.*, vol. 28, no. 1, pp. 19–31, Jan. 2010.
[3] J. E. Koroshetz, "Fiber lasers for lidar," in *Proc. Opt. Fiber Commun. Conf. Expo. Nat. Fiber Opt. Eng. Conf.*, Washington, DC, USA: Opt. Soc. Amer., 2005, Paper OFJ4.
[4] C. E. Wieman and L. Hollberg, "Using diode lasers for atomic physics," *Rev. Sci. Instrum.*, vol. 62, no. 1, pp. 1–20, 1991.
[5] L. He, Ş. K. Özdemir, J. Zhu, W. Kim, and L. Yang, "Detecting single viruses and nanoparticles using whispering gallery microlasers," *Nature Nanotechnol.*, vol. 6, no. 7, pp. 428–432, 2011.
[6] A. Hemmerich, D. McIntyre, D. Schropp, D. Meschede, and T. Hänsch, "Optically stabilized narrow linewidth semiconductor laser for high resolution spectroscopy," *Opt. Commun.*, vol. 75, no. 2, pp. 118–122, 1990.
[7] Y. Jiang *et al.*, "Making optical atomic clocks more stable with 10^{-16}-level laser stabilization," *Nature Photon.*, vol. 5, no. 3, pp. 158–161, 2011.
[8] C. Henry, "Theory of the linewidth of semiconductor lasers," *IEEE J. Quantum Electron.*, vol. QE-18, no. 2, pp. 259–264, Feb. 1982.
[9] C. Santis, S. Steger, Y. Vilenchik, A. Vasilyev, and A. Yariv, "High-coherence semiconductor lasers based on integral high-Q resonators in hybrid Si/III-V platforms," *Proc. Nat. Acad. Sci. U.S.A.*, vol. 111, no. 8, pp. 2879–2884, 2014.
[10] J. C. Hulme, J. K. Doylend, and J. E. Bowers, "Widely tunable Vernier ring laser on hybrid silicon," *Opt. Exp.*, vol. 21, no. 17, pp. 19 718–19 722, Aug. 2013.
[11] G. H. Duan *et al.*, "Hybrid III–V on silicon lasers for photonic integrated circuits on silicon," *IEEE J. Sel. Topics Quantum Electron.*, vol. 20, no. 4, pp. 158–170, Jul. 2014.
[12] S. Keyvaninia *et al.*, "Demonstration of a heterogeneously integrated III-V/SOI single wavelength tunable laser," *Opt. Exp.*, vol. 21, no. 3, pp. 3784–3792, Feb. 2013.
[13] T. Kita, R. Tang, and H. Yamada, "Compact silicon photonic wavelength-tunable laser diode with ultra-wide wavelength tuning range," *Appl. Phys. Lett.*, vol. 106, no. 11, 2015, Art. no. 111104.
[14] A. J. Zilkie *et al.*, "Power-efficient III-V/Silicon external cavity DBR lasers," *Opt. Exp.*, vol. 20, no. 21, pp. 23 456–23 462, Oct. 2012.
[15] T. Matsumoto *et al.*, "Narrow spectral linewidth full band tunable laser based on waveguide ring resonators with low power consumption," in *Proc. Opt. Fiber Commun. Conf.*, Washington, DC, USA: Opt. Soc. Amer., 2010, Paper OThQ5.
[16] D. de Felipe *et al.*, "Polymer-based external cavity lasers: Tuning efficiency, reliability, and polarization diversity," *IEEE Photon. Technol. Lett.*, vol. 26, no. 14, pp. 1391–1394, Jul. 2014.
[17] R. M. Oldenbeuving, E. J. Klein, H. L. Offerhaus, C. J. Lee, H. Song, and K.-J. Boller, "25 kHz narrow spectral bandwidth of a wavelength tunable diode laser with a short waveguide-based external cavity," *Laser Phys. Lett.*, vol. 10, no. 1, 2013, Art. no. 015804.
[18] Y. Fan *et al.*, "A hybrid semiconductor-glass waveguide laser," *Proc. SPIE*, vol. 9135, 2014, Art. no. 91351B.
[19] H. Ou, "Different index contrast silica-on-silicon waveguides by PECVD," *Electron. Lett.*, vol. 39, no. 2, pp. 212–213, Jan. 2003.
[20] K. Wörhoff, R. Heideman, A. Leinse, and M. Hoekman, "Triplex: A versatile dielectric photonic platform," *Adv. Opt. Technol.*, vol. 4, no. 2, pp. 189–207, 2015.
[21] L. Zhuang, D. Marpaung, M. Burla, W. Beeker, A. Leinse, and C. Roeloffzen, "Low-loss, high-index-contrast Si_3N_4/SiO_2 optical waveguides for optical delay lines in microwave photonics signal processing," *Opt. Exp.*, vol. 19, no. 23, pp. 23 162–23 170, Nov. 2011.
[22] J. F. Bauters *et al.*, "Planar waveguides with less than 0.1 dB/m propagation loss fabricated with wafer bonding," *Opt. Exp.*, vol. 19, no. 24, pp. 24 090–24 101, Nov. 2011.
[23] J. P. Epping *et al.*, "On-chip visible-to-infrared supercontinuum generation with more than 495 THz spectral bandwidth," *Opt. Exp.*, vol. 23, no. 15, pp. 19 596–19 604, Jul. 2015.
[24] C. G. H. Roeloffzen *et al.*, "Silicon nitride microwave photonic circuits," *Opt. Exp.*, vol. 21, no. 19, pp. 22 937–22 961, Sep. 2013.
[25] L. Zhuang, C. G. H. Roeloffzen, M. Hoekman, K.-J. Boller, and A. J. Lowery, "Programmable photonic signal processor chip for radiofrequency applications," *Optica*, vol. 2, no. 10, pp. 854–859, Oct. 2015.

[26] S. Tanaka, S.-H. Jeong, S. Sekiguchi, T. Kurahashi, Y. Tanaka, and K. Morito, "High-output-power, single-wavelength silicon hybrid laser using precise flip-chip bonding technology," *Opt. Exp.*, vol. 20, no. 27, pp. 28 057–28 069, Dec. 2012.
[27] N. Fujioka, T. Chu, and M. Ishizaka, "Compact and low power consumption hybrid integrated wavelength tunable laser module using silicon waveguide resonators," *J. Lightw. Technol.*, vol. 28, no. 21, pp. 3115–3120, Nov. 2010.
[28] K. Sato *et al.*, "Demonstration of silicon photonic hybrid ring-filter external cavity wavelength tunable lasers," in *Proc. Eur. Conf. Opt. Commun.*, Sep. 2015, pp. 1–3.
[29] B. Song, C. Stagarescu, S. Ristic, A. Behfar, and J. Klamkin, "3D integrated hybrid silicon laser," *Opt. Exp.*, vol. 24, no. 10, pp. 10 435–10 444, May 2016.
[30] D. Marcuse, "Reflection loss of laser mode from tilted end mirror," *J. Lightw. Technol.*, vol. 7, no. 2, pp. 336–339, Feb. 1989.
[31] L. A. Coldren, S. W. Corzine, and M. L. Massanovic, *A Phenomenological Approach to Diode Lasers*. Hoboken, NJ, USA: Wiley, 2012, pp. 45–90.
[32] N. Hosseini *et al.*, "Stress-optic modulator in triplex platform using a piezoelectric lead zirconate titanate (PZT) thin film," *Opt. Exp.*, vol. 23, no. 11, pp. 14 018–14 026, Jun. 2015.
[33] A. Nakayama, T. Okoshi, and K. Kikuchi, "Novel method for high resolution measurement of laser output spectrum," *Electron. Lett.*, vol. 16, no. 16, pp. 630–631, Jul. 1980.
[34] M. Osinski and J. Buus, "Linewidth broadening factor in semiconductor lasers—An overview," *IEEE J. Quantum Electron.*, vol. QE-23, no. 1, pp. 9–29, Jan. 1987.
[35] L. B. Mercer, "1/f frequency noise effects on self-heterodyne linewidth measurements," *J. Lightw. Technol.*, vol. 9, no. 4, pp. 485–493, Apr. 1991.
[36] M. Fleming and A. Mooradian, "Spectral characteristics of external-cavity controlled semiconductor lasers," *IEEE J. Quantum Electron.*, vol. QE-17, no. 1, pp. 44–59, Jan. 1981.
[37] S. D. Saliba and R. E. Scholten, "Linewidths below 100 kHz with external cavity diode lasers," *Appl. Opt.*, vol. 48, no. 36, pp. 6961–6966, Jul. 2014.
[38] A. J. Ward *et al.*, "Widely tunable DS-DBR laser with monolithically integrated SOA: design and performance," *IEEE J. Sel. Topics Quantum Electron.*, vol. 11, no. 1, pp. 149–156, Jan. 2005.
[39] Y. A. Akulova *et al.*, "Widely tunable electroabsorption-modulated sampled-grating DBR laser transmitter," *IEEE J. Sel. Topics Quantum Electron.*, vol. 8, no. 6, pp. 1349–1357, Nov. 2002.
[40] Z. Bian, B. Liu, and A. Shakouri, "InP-based passive ring-resonator-coupled lasers," *IEEE J. Quantum Electron.*, vol. 39, no. 7, pp. 859–865, Jul. 2003.
[41] K. Dridi, A. Benhsaien, J. Zhang, and T. J. Hall, "Narrow linewidth 1550 nm corrugated ridge waveguide DFB lasers," *IEEE Photon. Technol. Lett.*, vol. 26, no. 12, pp. 1192–1195, Jun. 2014.
[42] T. Kita, K. Nemoto, and H. Yamada, "Silicon photonic wavelength-tunable laser diode with asymmetric Mach–Zehnder interferometer," *IEEE J. Sel. Topics Quantum Electron.*, vol. 20, no. 4, pp. 344–349, Jul. 2014.